16th World Conference on Earthquake, 16WCEE 2017

Santiago Chile, January 9th to 13th 2017

Paper N° 1535 (Abstract ID)

Registration Code: S-L1462416001

Site Effect Study in Taiwan Using the Surface-Downhole Seismic Stations

Chun-Hsiang Kuo [(1)], Kuo-Liang Wen [(2)], Che-Min Lin [(3)]

[(1)] *Associate Research Fellow, National Center for Research on Earthquake Engineering, Taiwan,chkuo@ncree.narl.org.tw*
[(2)] *Professor, Department of Earth Sciences, National Central University, Taiwan,wenkl@earth.ncu.edu.tw*
[(3)] *Associate Research Fellow, National Center for Research on Earthquake Engineering, Taiwan,chkuo@ncree.narl.org.tw*

Abstract

A high-quality surface-downhole monitoring network is under construction in Taiwan by the Central Weather Bureau (CWB) since 2008. Twenty-nine surface-downhole stations had been installed in Taiwan until the end of 2013. Each station includes a pair of force balance accelerometers at the surface and the downhole, respectively, as well as one broadband velocity seismometer at the downhole. Earthquake records of those stations are very helpful in studying site effects in Taiwan. This study analyzes site effects including characteristics of Peak Ground Acceleration (PGA) and empirical transfer functions at fifteen of those stations using ground motion recordings from earthquakes with local magnitudes (M_L) of lager than four during 2012 and 2013. Moreover, all strong motion recordings of four large earthquakes ($M_L > 6$) are utilized to illustrate shake maps and magnitude differences for the surface and downhole locations. P-wave and S-wave velocity profiles at thirteen stations measured by a suspension PS-logging system are compiled by this study to calculate Vs30 at the sites. Site amplification factors of PGA are calculated by the ratio between the surface and the downhole recordings. The mean borehole amplification factors of PGA vary from 2 to an exaggerated value of 20 at different stations. In addition, a power-law relationship between PGAs at downhole and surface is evaluated to understand amplification variation with increasing PGA. Strong ground motions with and without site effects throughout Taiwan are able to be seen via the differences of the shake maps illustrated using the surface and downhole accelerations from four significant earthquakes with magnitude of larger than six in 2012 and 2013. The intensity differences at the surface and the downhole evidently indicate the site amplifications caused by the sediments during the large events. Empirical transfer functions derived by the single-station and the two-station methods at same stations show comparable dominant frequencies; however, the empirical transfer function from the two-station method shows clearer resonant peaks not only at fundamental frequencies but also at higher-mode of resonant frequencies. Moreover, this study further indicates that the local magnitudes calculated by surface recordings are obviously larger than those by downhole recordings. The differences are believed caused by the amplification of the sedimentary layers between the surface and downhole accelerometers. The difference of estimated local magnitudes is 0.38 in average for those large events.

Keywords: Peak Ground Acceleration; Site Effect; Local Magnitude; Taiwan

1. Introduction

Site effect is an important characteristic which caused by local unconsolidated sediments and usually results in significant enlargement of amplitudes and durations of seismic waves. Even though the source and path conditions are similar, two adjacent stations may lead to a large difference of seismic amplifications when the geological conditions are different [1, 2]. Typical cases of site amplifications for strong motions in Taiwan were observed inside the Taipei Basin during the events of 1986 and 2002 Hualien offshore earthquakes, as well as 1999 Chi-Chi earthquake. The soft sediments cover on the bedrock inside the basin caused significant amplifications on the seismic waves and then induced significant damages of buildings during these large earthquakes even though the epicentral distances to the Taipei Basin are all larger than 90 km.

The two-station [3] and single-station [4] methods are the most popular approaches to analyze the seismic site effect. The two-station approach is wildly used to estimate site amplification factors or horizontal to horizontal spectral ratio (HHSR), especially for seismic design codes [5, 6]. An adequate reference site, which has usually to be a hard rock site without obvious site effect, is essential for estimating site amplification factors in this approach, but usually difficult to be found in practice. The single-station method calculates a horizontal to vertical spectral ratio (HVSR) to assess the site effect and obtained a comparable result with the two-station methods [7]. The simple HVSR method is therefore becoming more and more popular in site effect studies [2, 8, 9].

A high density national strong ground motion network, that is, the so called TSMIP (Taiwan Strong Motion Instrumentation Program), has been installed in Taiwan since 1992 [10] and a total of more than 700 stations is working today. An investigation for the seismic site conditions at the free-field TSMIP stations was achieved for more than half stations in the past years [11, 12]. The data has been used for both local [13, 14, 15] and global [16, 17] strong motion and site effect studies as well as the seismic design code in Taiwan [18]. Several downhole seismic arrays were installed in Taiwan. The Lotung Large Scale Seismic Test (LLSST) project was carried out by the Taiwan Power Company (TaiPower) and the U.S. Electric Power Research Institute (EPRI) from 1985 to 1991 to install free-surface, downhole array, and structural accelerometers in Lotung Town, Ilan. Two downhole arrays consist of four downhole accelerometers, respectively, at the depths of 6, 11, 17, and 46 meters. A subsequent Hualien Large Scale Seismic Test (HLSST) project was carried out to construct free-surface, downhole array, and structural accelerometers in Hualien City in order to record near-field strong motions. A total of twelve downhole accelerometers were deployed in three downhole arrays at the depths of 5, 16, 26, and 53 meters. The LLSST and the HLSST arrays were a part of the networks of Strong Motion Array in Taiwan phase 1 (SMART1) and phase 2 (SMART2), respectively. The two networks played an important role in early strong ground motion monitoring and studies of Taiwan during 80s to 90s [19, 20, 21]. In order to understand the influence of the sedimentary layers for the propagation of seismic waves inside the Taipei Basin, the Central Geological Survey (CGS) and the Institute of Earth Sciences (IES), Academia Sinica successively deployed twelve strong motion downhole arrays inside the basin since 1991. Eight of those arrays are still monitoring today. Three to five accelerometers at surface and different depths were installed in each array. The strong motion recordings have been used by several studies on site effect and soil nonlinearity in the Taipei Basin [22, 23]. In addition, seven broadband downhole seismic arrays inside the Taipei Basin were constructed since 2005 in order to monitor micro-earthquakes. Each array consists of two broadband sensors at two different depths. During the 1999 Chi-Chi earthquake, damages occurred in the Taichung Harbor area due to the liquefaction effects caused by strong motions. The Center of Harbor and Marine Technology set up seismographers and piezometers at depths to monitor seismic waves and pore water pressures in several harbor areas [24]. The CGS and the National Center University (NCU) installed three downhole arrays in the Kaohsiung urban area to understand the site effect in the second metropolitan area in Taiwan. Those downhole arrays are able to help people to understand the local site effects in Taiwan especially in the Taipei Basin.

After the 1995 Hyogoken-Nanbu (Kobe) earthquake, the National Research Institute for Earth Science and Disaster Prevention (NIED) installed two national-wide strong motion seismograph networks, K-NET (kyoshin network) and KiK-net (kiban kyoshin network), which uniformly cover all Japan [25]. The K-NET is a free-field strong motions network whereas the KiK-net is an uphole/downhole observation network. Each station of the KiK-net consists of a strong motion seismograph at the surface, and a strong motion seismograph together with a

high sensitivity velocity seismograph (Hi-net) at the bottom of the observation boreholes. The uphole/downhole strong motion stations in Japan (KiK-net) provide very useful data for site effect studies [26, 27, 28].

In order to enhance ability of earthquake monitoring, location, and early warning, the Central Weather Bureau (CWB) continues upgrading seismographs as well as constructing a national network of surface-downhole stations for the whole of Taiwan. A total of 70 surface-downhole stations are expected to be installed under this project and 28 stations have accomplished until 2013. Each station includes a pair of force balance accelerometers at the surface and the downhole, respectively, as well as one broadband velocity seismometer at the downhole. The layout of the network is similar to the KiK-net of Japan. The strong motion data is suitable for studying site effect in Taiwan since both the accelerations at the surface and the bedrock are available via this network. Wang et al. [29] used the data to estimate the attenuation and velocity structures at 28 of those stations. Lai et al. [30] studied the kappa value in Taiwan using the borehole array data. In the current paper, we study the site effects by analyzing the site amplifications of PGA, empirical transfer functions, and the variations of local magnitudes using the strong motion data recorded by the surface-downhole network. Otherwise, both P-wave and S-wave velocity profiles at thirteen stations measured by a suspension PS-logging system were compiled by this study to calculate the Vs30.

2. Data acquisition and processing

A total of 28 surface-downhole stations have been installed by the CWB from 2008 to 2013. We selected 15 of those stations which have already recorded a number of data sets for the analysis on site effects. Otherwise, in order to illustrate shake maps for both surface and downhole, we employed 26 stations which recorded four large events; those data were also used to examine the difference of estimated local magnitudes. Both P-wave and S-wave velocity profiles were measured by a suspension PS-logging system at 13 of these stations and complied in this study.

2.1 The networks of surface-downhole stations

A network of surface-downhole stations is under construction by the CWB to enhance the ability of earthquake monitoring, location, and early warning. All stations of the network deliver real time digital data back to the Seismological Center in the CWB. 15 stations as shown in Fig. 1 were used in this paper to study the site effect of Taiwan. Each station includes a pair of force balance accelerometers at the surface and the downhole, respectively, as well as one broadband velocity seismometer at the downhole (Fig. 2). A 24-bit data recorder is placed at the surface to receive seismic data from the three sensors with a sampling rate of 100 Hz and then delivers back to the data center in the CWB by internet. Each of the observation boreholes is drilled into the bedrock, and thus the accelerometer pairs can therefore observe ground motions at both bedrock and surface. Among the 15 stations used in this study, the deepest observation borehole is 397 m depth at the CHY station whereas the shallowest borehole is 177 m depth at the ILA station. The downhole broadband seismometer situates at the deep bottom of observation boreholes to reduce artificial noises from the surface and therefore can observe high-quality data even from a small local earthquake. This study only used acceleration data for the site effect analyses. Fig. 2 shows a sketch for the configuration of equipments at a station.

2.2 Data processing

We acquired the seismic data of earthquakes with local magnitudes (M_L) of equal and larger than four which occurred in 2012 and 2013. The epicenter distributions are shown in Fig. 1. Earthquakes of different magnitudes are remarked by different sizes circles and a star. These symbols are filled by colors to express ranges of focal depths. However, the real time digital data stream sometimes becomes unstable during a strong shaking and the seismic data packets misses. Otherwise, square waves and abnormal noises are sometime involved in data sets. We excluded those data without signal and abnormal noises, and finally used a total number of 265 events for the analyses. The counts for those events with different magnitudes in different years used in this study were illustrated in Fig. 3. The directions of horizontal components of the downhole accelerometers have an offset from the north at several stations and thus we have to rotate the angle for these horizontal recordings. Finally, the baseline correction was done for all recordings by removing a mean value of the first three seconds.

Table 1 – Basic information for stations used in the study.

Station Code	Lon.	Lat.	Elevations	Angle	Vs30 (m/s)	Site Class
CHY	E 120.4325	N 23.4963	27 & -370	337	479	C
EGFH	E 121.4274	N 23.6688	132 & -163	0	na	na
HWA	E 121.6135	N 23.9751	16 & -273	144	301	D
ILA	E 121.7563	N 24.7638	7 & -170	0	233	D
LAY	E 121.5581	N 22.0373	324 & 128	0	na	na
NCUH	E 121.1849	N 24.9679	153 & -143	212	368	C
NMLH	E 120.7910	N 24.5372	201 & -95	0	498	C
NNSH	E 121.3829	N 24.4284	1106 & 813	88	538	C
NTC	E 121.8297	N 24.8544	4 & -288	0	400	C
NTS	E 121.4492	N 25.1644	16 & -276	0	276	D
OWD	E 121.1759	N 23.9545	1263 & 973	0	na	na
TTN	E 121.1549	N 22.7524	9 & -287	40	506	C
WCHH	E 120.5583	N 24.0795	34 & -262	185	500	C
WDLH	E 120.5381	N 23.6888	69 & -227	0	358	D
WJS	E 120.7279	N 23.8219	175 & -117	247	679	C

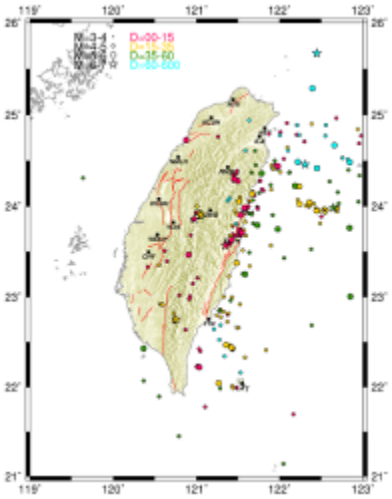

Fig. 1 – Locations of the 15 selected surface-downhole stations and the epicenter distribution of selected earthquakes (M_L >= 4). The black squares are locations of the stations together with the station codes. Magnitudes are remarked by different sizes of circles and a star, and the symbols are filled by colors to express ranges of the focal depths.

The basic information includes coordinates, elevations of surface and downhole accelerometers, offset angles of the downhole accelerometers, Vs30, and site classes for the 15 stations were listed in Table 1. The Vs30 values are obtained from a complied result of the PS-logging measurements. According to the results, all of the 15 stations belong to class C and D according to the Vs30 criterion of the NEHRP. Wang et al. [29]

calculated the average P-wave and S-wave velocities for 28 stations in their study. They compared the average S-wave velocities from their calculation with the complied results and the comparison showed the results are comparable at most stations except for the NNSH.

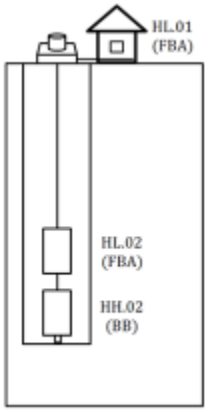

Fig. 2 – A sketch of the instrumentation configuration at a surface-downhole station. The acronyms of FBA and BB mean force balance accelerometer and broad-band sensor, respectively.

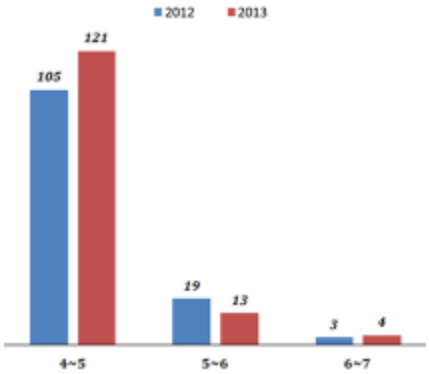

Fig. 3 – Counts for the earthquakes in the magnitude bins in the two years.

3. Methodologies

This study analyzed seismic site effect using peak accelerations and empirical transfer functions of the surface-downhole stations in both time and frequency domains.

3.1 Site amplification of PGA

We used the horizontal accelerations recorded by the surface and downhole stations to calculate the borehole amplification factor of PGA while seismic wave propagating from the bedrock to the surface. A geometric mean value of the north-south and east-west components is calculated as the horizontal PGA using Eq. (1).

$$\mathrm{PGA_H} = \sqrt{\mathrm{PGA_{NS}} \times \mathrm{PGA_{EW}}} \tag{1}$$

where the $\mathrm{PGA_H}$ is the horizontal PGA, and $\mathrm{PGA_{NS}}$ and $\mathrm{PGA_{EW}}$ are the PGAs of north-south and east-west directions, respectively.

A borehole amplification factor of PGA is subsequently calculated at a surface-downhole station by Eq. (2).

$$\mathrm{AMP} = {}^{\mathrm{PGA_S}}/_{\mathrm{PGA_D}} \tag{2}$$

where the AMP is the amplification factor, the PGA_S is the PGA of the surface acceleration, and the PGA_D is the PGA of the downhole acceleration. For each station, an amplification factor was calculated for every single event using Eq. (2) and then an average amplification factor for a station can therefore be derived as well as a standard deviation.

Otherwise, the PGA at the surface can be regarded as a function of the PGA at the downhole for each station. We adopt a power-law equation as shown in Eq. (3) to regress a relationship in order to understand the amplification variation with increasing PGA. This equation can represent the behavior of ground motion nonlinearity during a strong shaking.

$$PGA_S = a \times PGA_D{}^b \tag{3}$$

In the Eq. (3), a and b are the evaluated coefficients of the regression. The average amplification factor with a standard deviation and the power-law amplification relationship of PGA are derived in this study to understand the site effects at the 15 stations.

3.2 Empirical transfer function

Except for the estimation for PGA amplification in time domain, this study also implements an analysis of empirical transfer function to understand the entire site effect at different frequencies. A spectral ratio of a soil station and a rock station is usually regarded as a transfer function as a representative of site effect [3]. However, the used soil and rock stations must very close to each other and thus a suitable rock site is very difficult to be found in reality. A seismic time history is a convolution of source, path, and site effects and could be further considered as a product of those effects in frequency domain as shown in Eq. (4).

$$A(f) = E(f) \times P(f) \times S(f) \tag{4}$$

The A(f) is the spectrum of a seismic time history. E(f), P(f), and S(f) are the source, path, and site effects, respectively in the frequency domain. When the seismic data of an earthquake is used to analyze the site effect, once the hypocenter distance to a soil site is approximating to a reference rock site, the source and path effect can therefore be eliminated by using Eq. (5) to extract the transfer function of site effect ($S_T(f)$).

$$S_T(f) = A_S(f) / A_R(f) = S_S(f) / S_R(f) \tag{5}$$

The A_S and A_R are spectra of a soil site and a rock site. S_S and S_R are site effects at the soil site and rock site.

An alternative approach to estimate site effect is the so called horizontal to vertical spectral ratio method, i.e. the single station method. This method was proposed by Nakamura [4] as shown in Eq. (6) by examinations using both earthquake and microtremor data.

$$S_{TT}(f) = {S_{HS}(f)}\Big/{S_{VS}(f)} \tag{6}$$

In Eq. (6), S_{TT} is the spectral ratio of the horizontal (S_{HS}) and vertical spectra (S_{VS}) at surface. Nakamura [4] proposed the HVSR approach can eliminate the influence of Rayleigh wave that usually caused by near-surface soil layers. This approach works under two important assumptions: the effect of Rayleigh wave is equal in horizontal and vertical direction, and the horizontal and vertical spectra are equivalent at the downhole bedrock.

A reference rock site is not necessary in this method so that it is becoming more and more popular very quickly especially for applications on microtremor analysis. Lermo and Chávez-Garcia [7] further confirmed that this method can be applied to strong motion data. A horizontal spectrum used in two-station and single-station methods as shown in Eq. (5) and Eq. (6) is a quadratic mean of the Fourier spectra for north-south and east-west seismic data in this study.

3.3 Estimation of local magnitude (M_L)

Local magnitude, i.e. the Richter magnitude scale [31], is the official scale used by the CWB in Taiwan. The local magnitude is determined by the peak amplitude of seismic waves recorded by a Wood-Anderson seismometer. The seismic amplitudes recorded by the surface and downhole accelerometers at a station are quite different due to the site effect caused by the soft layers between the surface and bedrock and result in obviously divergence of the determined local magnitude. In Taiwan, the local magnitude is calculated by the three equations proposed by Shin [32] as in Eq. (7), (8), and (9).

$$\log A_0 = -0.00716 \times R - \log_{10}(R) - 0.39 \quad (7)$$

$$\log A_0 = -0.00261 \times R - 0.83 \times \log_{10}(R) - 1.07 \quad (8)$$

$$\log A_0 = -0.00326 \times R - 0.83 \times \log_{10}(R) - 1.01 \quad (9)$$

where A_0 is the peak amplitude of the reference earthquake recorded by a Wood-Anderson seismometer. R is the hypocentral distance for an earthquake. Eq. (7) and (8) are used for shallow earthquakes with a focal depth of ≦ 35 km; moreover, Eq. (7) is for near events with epicentral distances ≦80 km whereas Eq. (8) is for far events with epicentral distance > 80 km. Eq. (9) is used for deep earthquakes with a focal depth of larger than 35 km.

4. Site amplification analyses

The horizontal PGAs were calculated at both surface and downhole for events at each station and the distributions were shown in the left of Fig. 4. The relationships as shown in the right of Fig. 4 were evaluated by Eq. (3). Otherwise, the mean amplification factors at stations were calculated using Eq. (2) as well as the standard deviations. The PGA amplifications from the downhole bedrock to the surface as a factor and a power-law relation for each station a also provided in Table 2.

As for the empirical transfer functions, both two-station and single-station methods were adopted to evaluate the site effect at frequencies. The two-station method derives horizontal spectral ratio of the surface and the downhole, i.e. HHSR, whereas the single-station method derives horizontal to vertical spectral ratio at the surface. To avoid obvious nonlinearity during strong shaking, only the S-wave portions of PGA smaller than 50 gals were used to calculate the spectral ratios. The average two-station and single-station spectral ratios at each station were plotted together using a blue and a red curve respectively with plus and minus one standard deviation as shown in Fig 5.

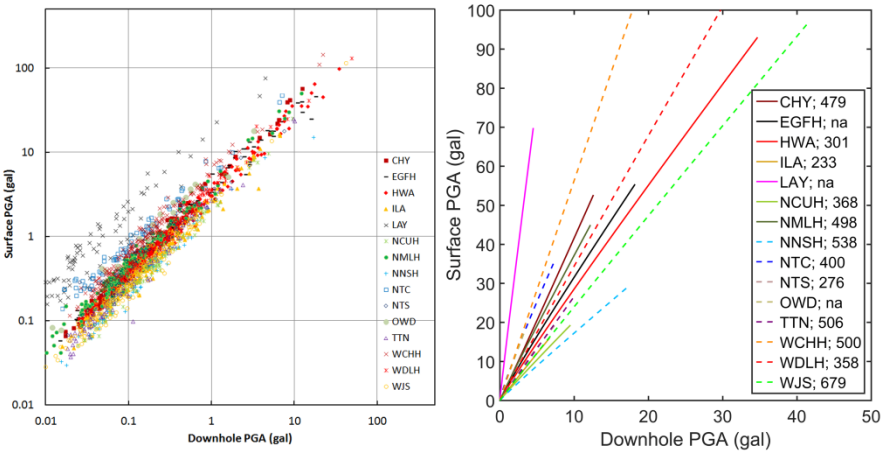

Fig. 4 – Distribution of PGA at downhole (x-axis) and surface (y-axis) and the regressed relationships.

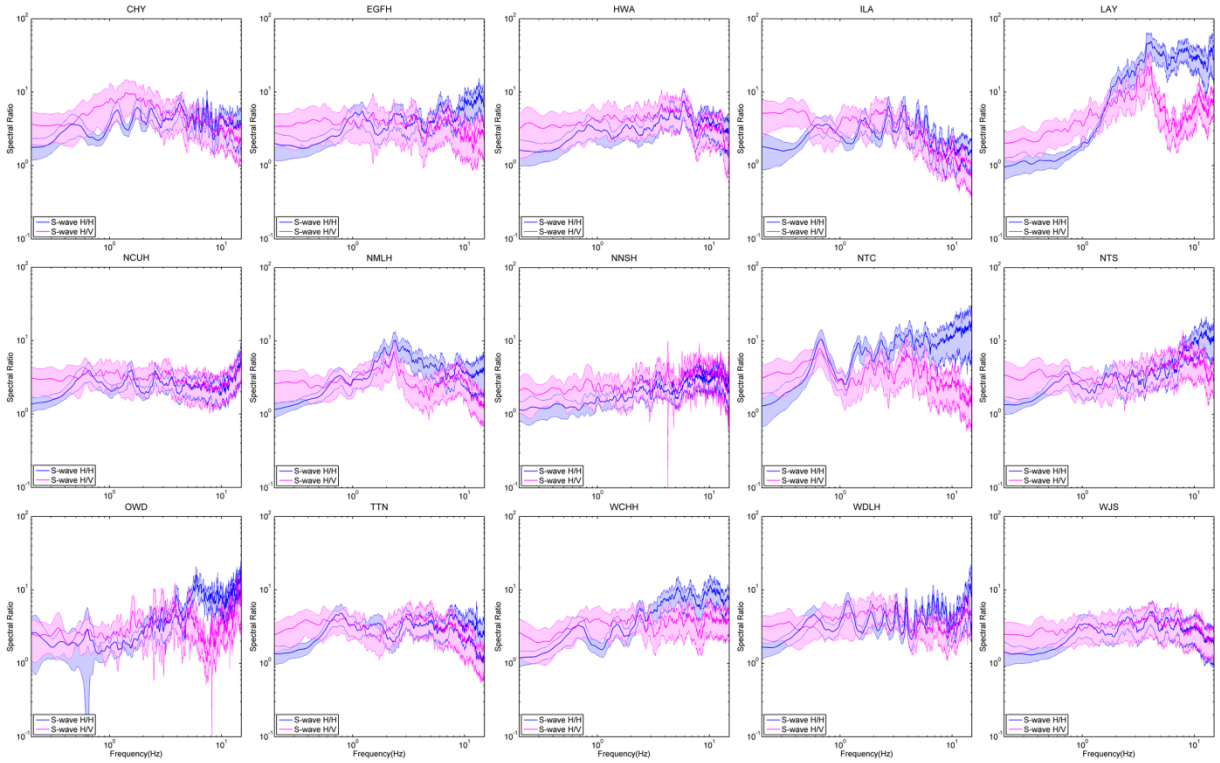

Fig. 5 – HHSR (blue) and HVSR (red) with one standard deviation ranges at each station.

Table 2 – PGA amplifications from the downhole to the surface as a foctor and a power-law relation at stations.

Station Code	AMP_{avg}	AMP_{std}	Relationship
CHY	3.88	0.58	$PGA_S=3.97\times PGA_D^{1.02}$
EGFH	3.93	0.87	$PGA_S=3.62\times PGA_D^{0.94}$
HWA	3.41	0.58	$PGA_S=3.20\times PGA_D^{0.95}$
ILA	2.59	0.47	$PGA_S=2.48\times PGA_D^{0.98}$
LAY	20.01	6.93	$PGA_S=16.47\times PGA_D^{0.96}$
NCUH	2.47	0.57	$PGA_S=2.22\times PGA_D^{0.96}$
NMLH	4.48	0.83	$PGA_S=4.07\times PGA_D^{0.96}$
NNSH	2.10	0.40	$PGA_S=1.89\times PGA_D^{0.96}$
NTC	7.81	1.95	$PGA_S=6.04\times PGA_D^{0.89}$
NTS	3.96	1.32	$PGA_S=3.18\times PGA_D^{0.90}$
OWD	6.45	1.30	$PGA_S=5.68\times PGA_D^{0.94}$
TTN	2.67	0.46	$PGA_S=2.66\times PGA_D^{1.00}$
WCHH	5.95	1.19	$PGA_S=5.76\times PGA_D^{0.99}$
WDLH	3.71	0.54	$PGA_S=3.60\times PGA_D^{0.98}$
WJS	2.69	0.55	$PGA_S=2.51\times PGA_D^{0.98}$

There are four large crustal earthquakes with local magnitudes of greater than 6 recorded by the surface-downhole network in 2012 and 2013. They are the Wutai earthquake (M_L6.4) occurred on February 26, 2012, the Nantou earthquake (M_L6.2) occurred on March 27, 2013, another Nantou earthquake (M_L6.5) occurred on June 6, 2013, and the Hualien earthquake (M_L6.4) occurred on October 31, 2013. The four earthquakes were felt throughout the whole of Taiwan, and thus provide an opportunity to see the divergence of the strong motions with and without site effects at the surface and at the downhole locations of the network. Shake maps of the four large earthquakes using the data from 26 stations of the surface-downhole network were therefore plotted in Fig. 6. The stations used in every single shake map are denoted as a black square, and the intensity according to the criterion used by the CWB was shown below. The legend shows the intensity grades from 0 (PGA < 0.8 gal) to 7 (PGA > 400 gal) in different colors. We used 15 stations to further analyze detail site effects in this study; however, all the surface-downhole stations recorded the four large earthquakes were used in plotting the shake maps. In order to assess the differences of the estimated M_L using the surface and the downhole data at each station, the same large earthquakes were used again. Fig. 7 shows the difference of estimated M_L at stations.

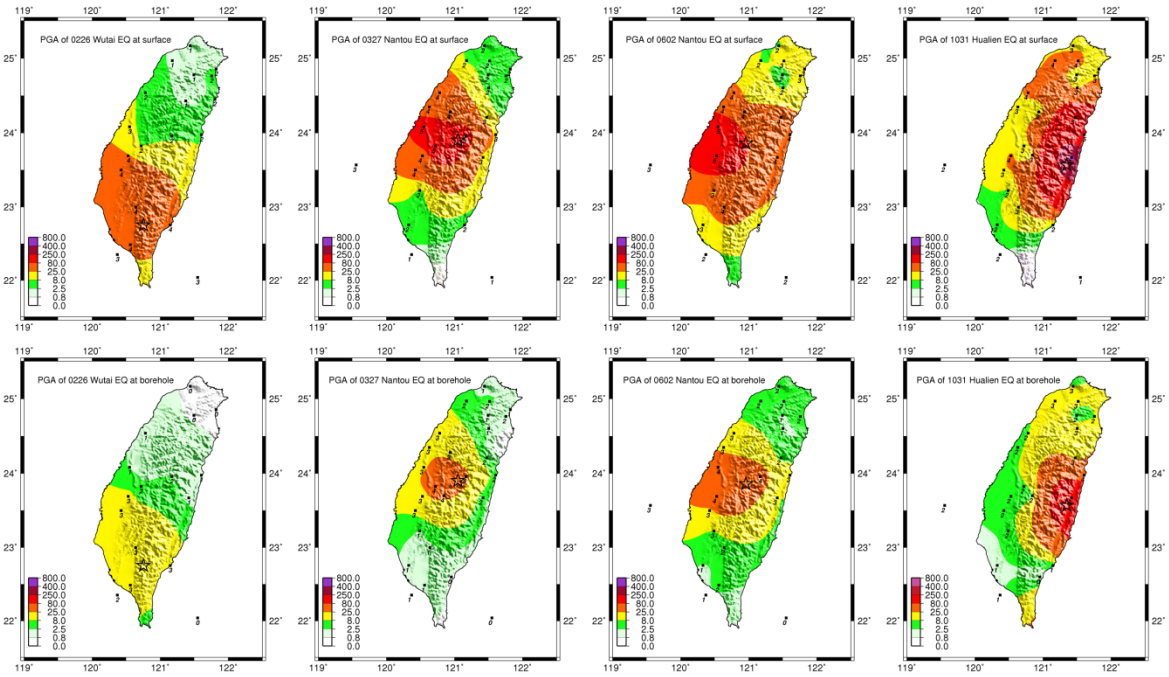

Fig. 6 – Shake maps at the surface and the downhole of the four large earthquakes occurred in 2012 and 2013.

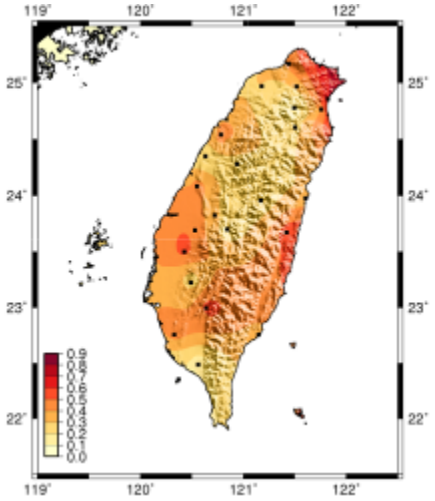

Fig. 7 – Difference of estimated M_L from the surface and the downhole at stations.

5. Discussions and conclusions

The analyzed results of PGA borehole amplifications as shown in Fig. 3 and Table 2 indicate that the borehole amplification factors for PGA are from twice (NNSH) to twenty times (LAY). However, the amplification factors at most stations are between 2 to 5 (Table 2). Because of downgoing wavefield, the amplifications estimated here are not really amplifications but pseudoresonances [33, 34]. The sedimentary layers are believed the major cause of the increase of PGA (seismic intensities) during an earthquake as shown in Fig. 6. The intensities at the surface are usually one grade greater than at the downhole in average. Such an amplification level is quite significant especially it is caused by very thin unconsolidated sediments (less than 400 m) in comparison to the focal or crustal depths (15 to 30 km). The intensity attenuated one grade with the horizontal distance increased around 40 km via the observations in Fig. 6. The site amplifications however show dramatically intensity increases along the vertical direction due to the non-isotropic of layered materials in this direction. The relationships between the downhole and surface PGA values show weak nonlinearity at most stations, because recordings with large PGA are still few for most stations.

The spectral ratios obtained by the two methods show comparable pattern and similar dominant frequencies. However, the HHSR and HVSR still have some differences in details. The HHSR not only indicates obvious peak at the dominant frequency but also shows clear peaks at higher resonant frequencies. The spectral ratios are helpful to understand site amplifications at frequencies. Station LAY as an example shows much greater amplification factor of PGA than other stations. The HHSR at LAY presents an extremely large amplification at frequencies higher than 3.5 Hz and it is believed the reason for the amplification of PGA. A vertical spectrum at the surface has lower values at low frequencies but has higher values at high frequencies relative to a horizontal spectrum at the downhole so that the HVSRs have higher ratio at low frequency and lower ratio at high frequency. The difference of frequency contents between horizontal and vertical spectra differentiates the HHSR and HVSR.

Fig. 6 shows shake maps of the strong motions at the surface and downhole, and therefore could be considered as with and without site effects. The shake map at the surface with site amplification obviously shows greater intensity than that at the downhole without site amplification. The same events with magnitudes of greater than 6 are used to find the differences of estimated local magnitudes due to the site effect. Local magnitude is derived from an instrument with a natural period of 0.8 sec (1.25 Hz) and thus can reflect the seismic response at an important frequency for engineering. As a result, the magnitude derived using the data at the surface is 0.38 larger than that using the downhole data in average. Fig. 7 indicates the stations located in plains and basins show larger difference than those at mountain area. However, large differences of magnitude to be found are the sites located near plain and basin edges. For examples, the magnitude differences are 0.7, 0.56, 0.53, and 0.54 at stations NTC, EGFH, CHY, and SLG, respectively. It indicates extremely seismic amplifications at a significant frequency (1.25 Hz) could occur at sites where obvious impedance between soft sediments and hard bedrocks exists. This result also implies that the estimated local magnitudes from the downhole seismometers may have to be corrected or the estimated magnitudes will be underestimated. An significant shift on consistency of earthquake catalog will be an important issue when more borehole records to be used, especially for estimation of b-value and seismic hazard assessment. That is the major reason for the preliminary analysis.

6. Acknowledgements

The authors would like to thank the CWB of Taiwan for providing the seismic data of the surface-downhole networks as well as technical assistances in determining the local magnitudes.

7. References

[1] Milne J. (1898): *Seismology*. London, K. Paul, Trench, Trubner & co.

[2] Wen KL, Lin CM, Chiang HJ, Kuo CH, Huang YC, Pu HC (2008): Effect of surface geology on ground motions: The case of station TAP056 - Chutzuhu Site. *Terrestrial Atmospheric and Oceanic Sciences*, **19** (5), 451-462.

[3] Borcherdt RD (1970): Effect of local geology on ground motion near San Francisco Bay. *Bulletin of Seismological Society of America*, **103** (2A), 1117-1129.

[4] Nakamura Y (1989): A method for dynamic characteristics estimation of subsurface using microtremor on the ground surface. *QR of RTRI*, **30** (1), 25-33.

[5] Borcherdt RD (1994): Estimates of site-dependent response spectra for design. *Earthquake Spectra*, **10** (4), 617-653.

[6] Borcherdt RD (2002): Empirical evidence for acceleration-dependent amplification factors. *Bulletin of Seismological Society of America*, **92** (2), 761-782.

[7] Lermo J, Chávez-Garcia FJ (1993): Site effect evaluation using spectral ratios with only one station. *Bulletin of Seismological Society of America*, **83**, 1574-1594.

[8] Bonilla LF, Steidl JH, Lindley GT, Tumarkin AG, Archuleta RJ (1997): Site amplification in the San Fernando Valley, California: variability of site-effect estimation using the S-wave, and H/V method. *Bulletin of Seismological Society of America*, **87**, 710-730.

[9] Kuo CH, Wen KL, Lin CM, Wen S., Huang JY (2015): Investigating near surface S-wave velocity properties using ambient noise in Southwestern Taiwan. *Terrestrial, Atmospheric and Oceanic Sciences*, **26** (2), 205-211.

[10] Liu KS, Shin TC, Tsai YB (1999): A free-field strong motion network in Taiwan: TSMIP. *Terrestrial Atmospheric and Oceanic Sciences*, **10** (2), 377-396.

[11] Kuo CH, Wen KL, Hsieh HH, Chang TM, Lin CM, Chen CT (2011): Evaluating empirical regression equations for Vs and estimating Vs30 in northeastern Taiwan. *Soil Dynamics and Earthquake Engineering*, **31** (3), 431-439.

[12] Kuo CH, Wen KL, Hsieh HH, Lin CM, Chang TM, Kuo KW (2012): Site Classification and Vs30 estimation of free-field TSMIP stations using the logging data of EGDT. *Engineering Geology*, **129-130**, 68-75.

[13] Shin TC, Chang CH, Pu HC, Lin HW, Leu PL (2013): The geophysical database management system in Taiwan. *Terrestrial Atmospheric and Oceanic Sciences*, **24** (1), 11-18.

[14] Wen KL, Peng HY (1998): Site effect analysis in the Taipei basin: Results from TSMIP network data. *Terrestrial Atmospheric and Oceanic Sciences*, **9** (4), 691-704.

[15] Sokolov V, Wenzel F, Wen KL, Jean WY (2012): On the influence of site conditions and earthquake magnitude on ground-motion within-earthquake correlation: analysis of PGA data from TSMIP (Taiwan) network. *Bulletin Earthquake Engineering*, **10** (5), 1401-1429.

[16] Ancheta TD, Darragh RB, Stewart JP, Seyhan E, Silva WJ, Chiou BSJ, Wooddell KE, Graves RW, Kottke AR, Boore DM, Kishida T, Donahue JL (2014): NGA-West2 Database. *Earthquake Spectra*, **30** (3), 989-1005.

[17] Du W, Wang G (2013): Intra-event spatial correlations for cumulative absolute velocity, arias intensity, and spectral accelerations based on region site conditions. *Bulletin of Seismological Society of America*, **103** (2A), 1117-1129.

[18] CPA (2011): *Seismic Design Code and Commentary for Buildings*. Construction and Planning Agency, Ministry of Interior Affair, 2011 edition. (In Chinese)

[19] Wen KL, Yeh YT, and Huang WG (1992): Effects of alluvial basin on strong ground motions. *Bulletin of Seismological Society of America*, **82** (2), 1124-1133.

[20] Beresnev IA, Wen KL, Yeh YT (1994): Source, path, and site effects on dominant frequency and spatial variation of strong ground motion recorded by SMART1 and SMART2 arrays in Taiwan. *Earthquake Engineering & Structural Dynamics*, **23** (6), 583-597.

[21] Wen KL, Beresnev IA, Yeh YT (1994): Non-linear soil amplification inferred from downhole strong seismic motion data. *Geophysical Research Letters*, **21** (24), 2625-2628.

[22] Wen KL, Fei LY, Peng HY, Liu CC (1995): Site effect analysis from the records of the Wuku downhole array. *Terrestrial Atmospheric and Oceanic Sciences*, **6** (2), 285-298.

[23] Huang WG, Huang BS, Wang JH, Chen KC, Wen KL, Tsao SH, Hsieh YC, Chen CH (2010): Seismic observation in the Taipei metropolitan area using a downhole network. *Terrestrial Atmospheric and Oceanic Sciences*, **21** (3), 615-625.

[24] Chen KC, Lee FB, Chen JF, Hsieh MJ, Lai RI (2005): Geotechnical Monitoring and Measures against Liquefaction at Harbor Areas (3/3). *MOTC-IOT-93-H1DA003*, Harbor & Marine Technology Center, Institute of Transportation, Ministry of Transportation and Communications, Taipei, Taiwan. (In Chinese with English abstract)

[25] Aoi S, Kunugi T, Fujiwara H (2004): Strong-motion seismograph network operated by NIED: K-NET and KiK-net. *Journal of Japan Association for Earthquake Engineering*, **4** (3), 65-74.

[26] Kim B, Hashash Y.M.A (2013): Site response analysis using downhole array recordings during the March 2011 Tohoku-Oki earthquake and the effect of long-duration ground motions. *Earthquake Spectra*, **29** (S1), S37-S54.

[27] Assimaki D, Li W, Steidl J.H., Tsuda K (2008): Site amplification and attenuation via downhole array seismogram inversion: a comparative study of the 2003 Miyagi-Oki aftershock sequence. *Bulletin of Seismological Society of America*, **98** (1), 301-330.

[28] Heloise C, Bard P.Y., Rodriguez-Marek A (2012): Site effect assessment using KiK-net data: part 1. a simple correction procedure for surface/downhole spectral ratios. *Bulletin of Earthquake Engineering*, **10**, 421-448.

[29] Wang YJ, Ma KF, Wu SK, Hsu HJ, Hsiao WC (2016): Near-surface attenuation and velocity structures in Taiwan from comparison of wellhead and borehole recordings. *Terrestrial Atmosphere Oceanic Science* (in press).

[30] Lai TS, Mittal H, Chao WA, Wu YM (2016): A study on Kappa value in Taiwan using borehole seismic array. *Bulletin of Seismological Society of America*. (accepted)

[31] Richter CF (1935): An instrumental earthquake magnitude scale. *Bulletin of Seismological Society of America*, **25** (1), 1-32.

[32] Shin TC (1993): The calculation of local magnitude from the simulated Wood-Anderson seismograms of the short-period seismograms in the Taiwan area. *Terrestrial Atmospheric and Oceanic Sciences*, **4** (2), 155-170.

[33] Steidl JH, Tumarkin AG, Archuleta RJ (1996): What is a reference site?. *Bulletin of Seismological Society of America*, **86** (6), 1733-1748.

[34] Bonilla LF, Steidl JH, Gariel JC, Archuleta RJ (2002): Boreholw response studies at the Garner Valley Downhole Array, Southern California. *Bulletin of Seismological Society of America*, **92**(8), 3165-3179.